2016 23rd International Conference on Pattern Recognition (ICPR)
Cancún Center, Cancún, México, December 4-8, 2016

Multi-scale Underwater Descattering

Cosmin Ancuti*‡, Codruta O. Ancuti†‡, Christophe De Vleeschouwer*, Rafael Garcia† and Alan C. Bovik§
*ICTEAM, Universite Catholique de Louvain, Belgium
†Computer Vision and Robotics Group, University of Girona, Spain
‡MEO, Universitatea Politehnica Timisoara, Romania
§Department of Electrical and Computer Engineering, The University of Texas at Austin, USA

***Abstract*—Underwater images suffer from severe perceptual/visual degradation, due to the dense and non-uniform medium, causing scattering and attenuation of the propagated light that is sensed. Typical restoration methods rely on the popular Dark Channel Prior to estimate the light attenuation factor, and subtract the back-scattered light influence to invert the underwater imaging model. However, as a consequence of using approximate and global estimates of the back-scattered light, most existing single-image underwater descattering techniques perform poorly when restoring non-uniformly illuminated scenes. To mitigate this problem, we introduce a novel approach that estimates the back-scattered light locally, based on the observation of a neighborhood around the pixel of interest. To circumvent issue related to selection of the neighborhood size, we propose to fuse the images obtained over both small and large neighborhoods, each capturing distinct features from the input image. In addition, the Laplacian of the original image is provided as a third input to the fusion process, to enhance texture details in the reconstructed image. These three derived inputs are seamlessly blended via a multi-scale fusion approach, using saliency, contrast, and saturation metrics to weight each input. We perform an extensive qualitative and quantitative evaluation against several specialized techniques. In addition to its simplicity, our method outperforms the previous art on extreme underwater cases of artificial ambient illumination and high water turbidity.**

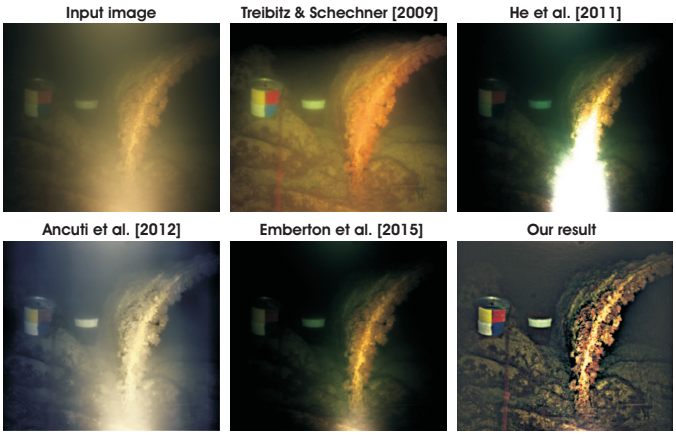

Fig. 1. ***Underwater scene restoration.*** Special-purpose single-image dehazing method of He et al. [21] and also specialized underwater dehazing methods of Ancuti et al. [15] and Emberton et al. [20] are limited in their ability to recover the visibility of challenging underwater scenes. While the polarization-based technique (uses multiple images) of Treibitz and Schechner [7] is competitive, our approach better restores both color and contrast (local and global) in the underwater image.

I. Introduction

Underwater imaging is required in many applications [1] such as control of underwater vehicles [2], marine biology research [3], inspection of the underwater infrastructure [4] and archeology [5]. However, as compared with computer vision and image processing applications in the surface environment, image analysis underwater is a much more difficult problem, awing to the dense and strongly non-uniform medium where light scatters, i.e. is forced to deviate from its straight trajectory. The poor visual quality of underwater images is mainly due to the attenuation and back-scattering of illumination sources. Back-scattering refers to the diffuse reflection of light, in the direction from which it emanated.

Early underwater imaging techniques employed specialized hardware [6] and multiple images polarized over diverse angles [7], resulting in either expensive or impractical acquisition systems. Recently, inspired by outdoor dehazing [8], [9], [10], [11], [12], [13], [14], several single-image based underwater image enhancement solutions [15], [16], [17], [18], [19], [20] have been introduced. Chiang and Chen [17] first segment the foreground of the scene based on a depth estimate resulting from the Dark Channel Prior (DCP) [9], [21], then perform color correction based on the amount of attenuation expected for each light wavelength. Galdran et al. [19] introduce the Red Channel to recover colors associated with short wavelengths in underwater. Ancuti et al. [15] derives two color corrected inputs and merge them using a multi-scale fusion technique [22]. While the technique proposed in this paper is also based on a multi-scale fusion strategy, here, we derive three distinct inputs that are robust in the presence of highly non-uniform illumination of the scenes (see Fig. 1).

Despite these recent efforts, existing single-image underwater techniques exhibit significant limitations in the presence of turbulent water and/or artificial ambient illumination (see Fig. 1). This is mainly due to poor estimation of the back-scattered light, which is generally assumed to be uniform over the entire image. A unique global value of back-scattered light is only valid in relatively simple underwater scenes having nearly uniform illumination, as is encountered in most outdoor hazy scenes.

In this paper we introduce a novel approach based on local estimation of the back-scattering influence. Following the optical underwater model [23], we first compute the back-scattered light by searching for the brightest location along each image patch. By simply inverting the optical model using

978-1-5090-4846-5/16/$31.00 ©2016 IEEE

our local estimate of the back-scattered light, we are able to obtain a good degree of visual restoration, even on in extreme underwater scenes. Since the size of the patch should depend on multiple parameters characterizing the captured underwater scene (e.g. the dimensions and colors of objects in the scenes, nature of the ambient light, non-uniform illumination) we use a variety (only two in practice) of patch dimensions, each size supporting the recovery of distinct and complementary features of the scene. Specifically, a first image is derived using a smaller patch to better restore the contrast, while a second image is derived based on a large patch size, which makes it possible to consistently recover regional color. To highlight and enhance the fine details of the initial image, we also compute its discrete Laplacian. These three images derived from the original image, guided by several quality measures, are seamlessly blended using a multi-scale fusion approach [22].

We perform an extensive qualitative and quantitative evaluation against several existing specialized techniques. Despite its simplicity, our method proves quite robust and produces competitive results on highly opaque and non-uniformly illuminated underwater scenes.

II. Underwater Image Formation

Based on the well-known optical model of McGlamery [23], in the underwater medium the total radiance of an image $\mathcal{I}$ that reaches the observer is due to three additive components: a *direct component* E_D, a *forward-scattering* component E_{FS} and a *back-scattering* component E_{BS}. These components mainly result from the radiances of objects in the scene and the ambient light.

The *direct component* E_D represents the attenuated version (with distance) of the reflected light, and is expressed at each image coordinate x as:

$$E_D(x) = J(x)e^{-\eta d(x)} = J(x)t(x) \tag{1}$$

where $J(x)$ is the radiance of the object, $d(x)$ is the distance between the observer and the object, and η is the attenuation coefficient. The exponential term $e^{-\eta d(x)}$ is also known as the transmission t through the underwater medium.

Forward-scattering E_{FS}, is the deflection of a portion of the incident light. In general, it is associated with a small fraction of the overall image degradation process.

Back-scattering, also known as the *veiling light* [24], is the principal cause for the loss of contrast and the color shifting of underwater images. For reasonable distances (between 3-10 m) this component may be expressed as [24]:

$$E_{BS}(x) = B_\infty(1 - e^{-\eta d(x)}) \tag{2}$$

where B_∞ is a scalar known as the *back-scattered light* or the *water background* [25]. Assuming homogeneous lighting along the line of sight, this component may be regarded as originating from an equivalent sources at infinity [24].

Incorporating these additive components and ignoring the forward scattering component, the simplified underwater optical model employed in most existing descattering techniques, becomes:

$$\begin{aligned}\mathcal{I}(x) &= J(x)e^{-\eta d(x)} + B_\infty(1 - e^{-\eta d(x)}) \\ &= J(x)t(x) + B_\infty(1 - t(x))\end{aligned} \tag{3}$$

Since the underwater camera model (3) has a similar form as the optical model of Koschmieder [26], used to characterize the propagation of light in the atmosphere, many recent approaches have proposed to restore underwater images based on the extension of popular and effective outdoor dehazing methods. For instance, Chiang and Chen [17] estimate the rough depth of the underwater scene based on the Dark Channel Prior (DCP) [21], then adjust the bluish tone based on a wavelength compensation strategy. Similarly, Galdran et al. [19] propose a variation of DCP, in which the so-called Red Channel is used to recover colors associated with short wavelengths underwater.

However, these outdoor dehazing-derived techniques appear to be successful mostly on less challenging underwater scenes. They generally assume shallow underwater scenes with relatively transparent water and effective ambient illumination. These cases, which are indeed similar to outdoor hazy scenes, represent only a fraction of the underwater imaging problem. At greater depths and under artificial illumination, the visibility degradation is more critical and dehazing approaches suffer from important limitations when restoring contrast and color (see Fig. 1). We explain in the rest of the paper how (3) can be inverted in the case of arbitrary underwater scenes.

III. Estimation of Transmission and Back-scattering

There are two unknowns in the image acquisition model defined by equation (3): the transmission map $t(x)$ and the back-scattered light B_∞.

A. Transmission Estimation

Following recent techniques, we approximate the transmission $t(x)$ based on the Dark Channel Prior (DCP) of He et al. [21]. This prior assumes that natural objects have a weak reflectance in one of the color channels. In other words, the direct radiance is small, or dark, in at least one of the R,G,B color channels. Given this assumption, the transmission map, $t(x)$, can be estimated from the weakest color over a neighborhood of x. Formally, the DCP asserts that $\min_{y\in\Omega(x)}\left(\min_{c\in r,g,b}\mathcal{J}^c/{B_\infty}^c\right) = 0$. Hence, the optical model (3) yields:

$$t(x) = 1 - \min_{y\in\Omega(x)}\left(\min_{c\in r,g,b}\mathcal{I}^c(x)/{B_\infty}^c\right) \tag{4}$$

where $\Omega(x)$ represents a local patch centered at x.

In practice, $t(x)$ is reasonably well approximated by replacing the back-scatteredlight B_∞ with the maximal color intensity vector $[1, 1, 1]$, so that:

$$t(x) \approx 1 - \min_{y\in\Omega(x)}\left(\min_{c\in r,g,b}\mathcal{I}^c(x)\right) \tag{5}$$

In the literature [21], the term $\min_{y\in\Omega(x)}\left(\min_{c\in r,g,b}\mathcal{I}^c(x)\right)$ is referred to as the dark channel image, and is denoted $\mathcal{I}_{\mathcal{DC}}(x)$.

B. Global Back-scattering Estimation

The other unknown that is required to invert the optical underwater acquisition model is the back-scattered light B_∞, which represents the light that is scattered back by floating particles. This is the main cause of contrast and color degradation in underwater images.

Most existing underwater descattering strategies compute a global value of the back-scattered light over the entire image. Similar to what is done in outdoor dehazing [8], [27], [21], this value is usually determined in the brightest region of the dark channel image [18], [19]. This is because, when $I_{DC}(x)\rightarrow 1$, equation (5) implies that $t(x)\rightarrow 0$, and the optical model then states that $I(x)\rightarrow B_\infty$.

Formally, following He et al. [21], the back-scattered light can be estimated as:

$$\begin{aligned} &B_\infty = \mathcal{I}(y*),\ with \\ &y* = \underset{y|\mathcal{I}_{\mathcal{DC}}(y)>{\mathcal{I}_{\mathcal{DC}}}^{99.9}}{\textbf{\textit{arg max}}} \left(\mathcal{I}^r(y)+\mathcal{I}^g(y)+\mathcal{I}^b(y)\right) \end{aligned} \tag{6}$$

In this equation, $y*$ denotes the location of the brightest pixel among those pixels whose dark channel value lies above the 99.9^{th} percentile ${\mathcal{I}_{\mathcal{DC}}}^{99.9}$, while r, g, b refer to the red, green and blue color components, respectively. The above equation can be written on a color component basis, as:

$$B^c_\infty \simeq \max_{y|\mathcal{I}_{\mathcal{DC}}(y)>{\mathcal{I}_{\mathcal{DC}}}^{99.9}} \mathcal{I}^c(y), \tag{7}$$

where c corresponds to each one of the color channels ($c=[r,g,b]$) and ${\mathcal{I}_{\mathcal{DC}}}^{99.9}$ denotes the 99.9^{th} percentile of the dark channel over the entire image.

To achieve robustness to specular reflections and glowing effects that tend to mislead the color estimator defined by (6) and (7) in underwater mediums [28], we introduce an alternative definition of the global back-scattered light estimator that finds and uses the minimum of $\mathcal{I}^c$ over a small neighborhood around y. Formally, we define:

$$B^c_{G_\infty} = \max_{y\in M^I_{DC}} \left(\min_{z\in\Omega(y)} \mathcal{I}^c(z)\right) \tag{8}$$

where $\Omega(y)$ is a neighborhood around y, and M^I_{DC} is the set of locations in the image support $\mathcal{I}$ where the dark channel reaches its global maximum value ${\mathcal{I}_{\mathcal{DC}}}^{max}$, i.e. $M^I_{DC}=\{y|\mathcal{I}_{\mathcal{DC}}(y)=\mathcal{I}^{max}_{DC}\}$. Hence, instead of keeping an arbitrary 99.9^{th} percentile, we retain the entire set of coordinates where $\mathcal{I}_{\mathcal{DC}}$ is maximum. Since the dark channel $\mathcal{I}_{\mathcal{DC}}(x)$ is defined based on minimization over a patch, M^I_{DC} always include multiple locations. Our validations reveal that using M^I_{DC} (instead of the 99.9^{th} percentile), does not negatively impact the global estimation. Moreover, it makes the expression easier to generalize to a local estimator, as explained in the next sub-section. Before moving to our proposed local estimator, we first point out the equivalence and the limitations of the two global estimators defined by (6) and (8). As shown in Fig. 2, expressions (6) and (8) yield comparable results when inverting the optical model (3), and provide satisfying approximations in an underwater medium with relatively uniform illumination. However, as illustrated in Fig. 3, both global estimators fail in the presence of non-uniform illumination.

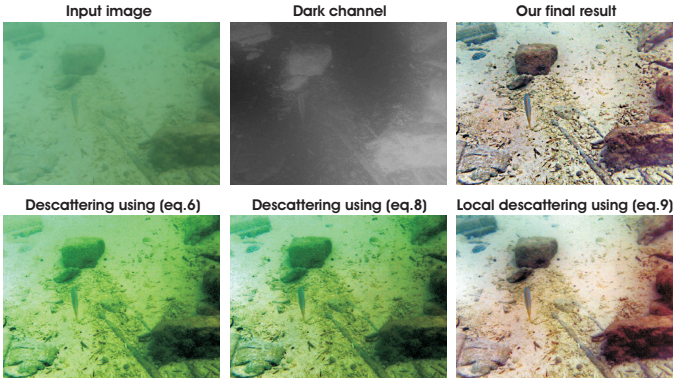

Fig. 2. ***Global vs. Local descattering in uniform underwater medium.*** Compared with global estimates of the back-scattering, the strategy based on our patch-based estimation of back-scattering allows for better restoration of visibility, even in a uniform underwater medium.

C. Local Back-scattering Estimation

The problem of non-uniform back-scattering becomes especially challenging at greater depths, where artificial illumination is required. Local estimation of the back-scattered light has been recently considered for underwater dehazing by Emberton et al. [20]. They designed a hierarchical rank-based method, using a set of features to find those image regions which are the most haze-opaque. Here, we introduce an alternative approach to be able to adapt locally to the back-scattered light. Our proposal achieves visually improved descattering, as attested by the results presented in Fig. 5 and Fig. 6. Starting from equation (8), we propose to compute the back-scattered light at location x as:

$$B^c_{L_\infty}(x) = \max_{y\in M^{\Psi(x)}_{DC}} \left(\min_{z\in\Omega(y)} \mathcal{I}^c(z)\right) \tag{9}$$

where $\Psi(x)$ is a square patch centered at x. As for the global estimator, $M^{\Psi(x)}_{DC}$ denotes the set of positions in $\Psi(x)$ where the dark channel is maximum, i.e. reaches the value of its local maximum over $\Psi(x)$. In practice, the patch Ψ is typically larger than Ω. We use a default value of 2 for the ratio between the sizes of the Ψ and Ω patches. A higher ratio is recommended for processing underwater scenes with relatively uniform illumination and less turbidity. As shown in Figs. 2 and 3, the contrast and color are better recovered when inverting the underwater acquisition model based on our proposed local back-scattering estimator as compared to inverting based on the global method.

IV. Descattering by Multi-scale Fusion

A critical issue related to equation (9) lies in the selection of the patch size Ω. Using a large patch tends to reduce the

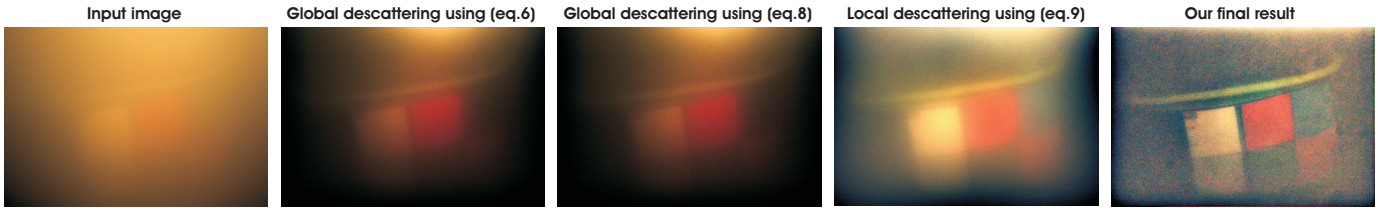

Fig. 3. ***Global vs. Local descattering in non-uniform underwater medium.*** While global estimation of the back-scattering performs poorly in such challenging underwater scenes, the same restoration strategy yields consistent improvement by using our local estimation of back-scattering.

impact of specular reflections and glowing effects in underwater mediums, but also tends to preserve the undesirable hazy appearance with reduced improvement of the contrast as compared to using a smaller patch (see Fig. 4).

Inspired by our previous approach [15], of keeping the best from among small and large patches, we propose a multi-scale fusion approach to blend the images obtained with both a large and a small patch size. Image fusion is a well-known process that aims to optimize the appearance of a reconstructed scene by effectively blending the information of multiple inputs. Multi-scale fusion based on the Laplacian pyramid [22] has been shown to be effective for various computational imaging applications such as extended depth-of-field [29], image editing [30], image compositing [31], HDR imaging [32], image decolorization [33], [34] and single image dehazing [35], [11]. The fusion process is typically guided by several spatial weight maps that capture, the contribution of each input image to the final output. These weight maps typically assess contrast, saturation and saliency.

A. Inputs

Our fusion technique is a single image-based approach that derives several inputs from an original underwater input. First, we derive inputs based on our patch-based estimation of the back-scattering influence, as discussed in the previous section. We observed that choosing different patch sizes yields good recovery either of contrast (small patch) or color (large patch). Since we cannot simultaneously obtain good restoration of both of these important factors using a single patch size, we derive two inputs generated using two different patch sizes.

Using a large patch size better restores color while choosing a small patch size is more effective in restoration of the visibility (global contrast).

As a result, to remove most of the hazy appearance of the underwater images we derive a **first input** based on our local back-scattering estimation (9) computed using a small patch size (e.g. 20×20 for an image of size 800×600). Moreover, to better restore color we derive, using the same approach, a **second input** using a larger patch size (e.g. 60×60 for an image of size 800×600). Our experiments have revealed that considering additional patch sizes does not deliver any added value to the reconstruction.

However, as can be seen in Fig. 4, those two inputs fail to capture the finest detail. To also transfer this important information to the final result we derive a **third input** which is the discrete Laplacian of the original image.

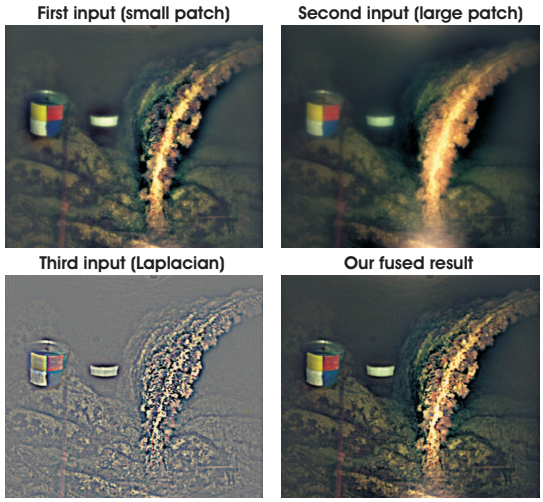

Fig. 4. ***Derived Inputs.*** Our single image-based fusion algorithm considers three derived inputs. The first one estimates back-scattering on a small patch and removes most of the hazy appearance, the second estimates back-scattering on a large patch and primarily restores the color, and the third computes the Laplacian of the original to preserve fine details.

B. Weight Maps

Inspired by our previous fusion underwater approach [15], we derive three weight maps. This ensures that locations of high contrast or high saliency will receive greater emphasis in the fusion process.

Local contrast weight detects the degree of local variation of each derived input. Estimated similarly as in [32], [11] it assigns high values to edges and texture variations, by computing the L_1 norm of Laplacian filter applied to the luminance channels of each input .

Saturation weight map is motivated by the fact that humans generally prefer images containing a high level of color saturation. This measure is computed as the standard deviation across color channels at each pixel coordinate.

Saliency weight map advantages the most conspicuous regions of an image. This weight is computed using the saliency technique of Achanta et al. [36].

Each of those weight maps is scaled so that its range lies between 0 and 1. A pixelwise product of those three normalized maps is then used to derive a single map.

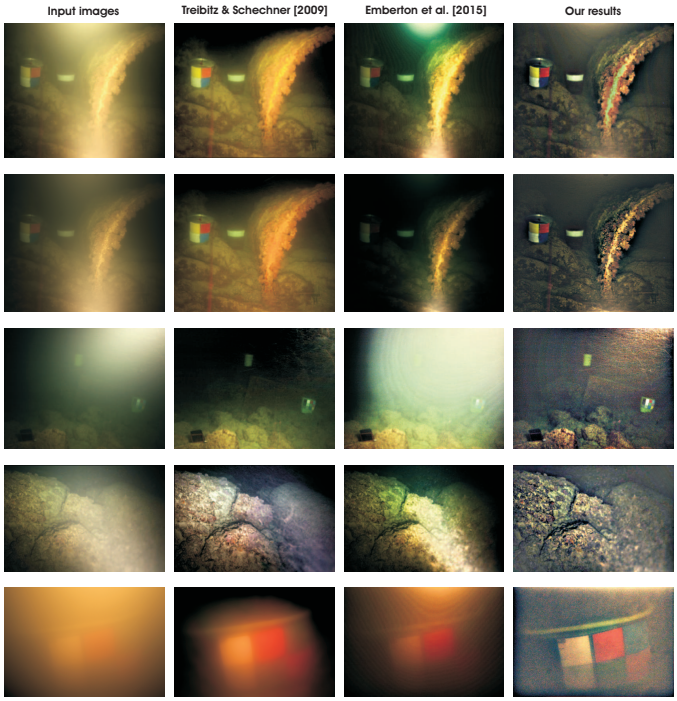

Fig. 5. Comparative results on underwater scenes with non-uniform lightning.

C. Multi-scale Fusion

Since naive fusion implementation (directly blending the inputs and weight maps) causes unpleasing halo artifacts [15], we instead employ the multi-scale Laplacian decomposition [22]. Using the same number of levels, the Gaussian and Laplacian pyramids are independently fused at each level:

$$\mathcal{R}_l(x) = \sum_k G_l\left\{\bar{\mathcal{W}}^k(x)\right\} L_l\left\{\mathcal{I}_k(x)\right\} \tag{10}$$

where l is the level of the pyramid, k is the input index, $L\{\mathcal{I}\}$ denotes the Laplacian of the input $\mathcal{I}$, and $G\{\bar{\mathcal{W}}\}$ is the Gaussian-smoothed normalized weight map $\bar{\mathcal{W}}$. Here, the normalization ensures that the sum of weights over the three inputs is equal to unity at each pixel. The final fused result $\mathcal{R}$ is processed by summing the contributions from all the computed levels of the pyramid.

V. Results and Discussion

Our approach has been extensively tested on a large number of underwater images captured in various environments. We compared our results with those produced by recent special-purpose underwater enhancment methods [16], [18], [19], [20] and also with the seminal dehazing techniques of He et al. [21].

Fig. 5 presents several images taken from the work of Tali and Schechner [7]. These images are artificially illuminated and, due to multiple scattering process [7], the light is non-uniformly spread over the entire scene. Even if Emberton et al. [20] estimates back-scattering influence locally, it fails to restore both the contrast and the color of the scene. As shown also in Fig. 1, outdoor dehazing techniques [21] exhibit similar limitations. On the other hand, our approach performs considerably better than the polarization approach of Treibitz and Schechner [7] that employs two images (taken with different states of the light-source polarizer).

Fig. 6 completes the comparative analysis by presenting the results obtained when restoring underwater scenes with relatively uniform illumination. In this particular case, existing underwater approaches [16], [18], [19], [20] generally lead to satisfying results. For this less challenging case, we performed a quantitative evaluation. We considered the same set of 10 underwater images used by Emberton et al. [20] to assess the various underwater techniques [19], [15], [17], [18].

As quantitative assessment metrics, we employed two contrast-based measurements: the hazy visibility metric (VM) [37] also used in [20], and the recent patch-based contrast quality index (PCQI) of Wang et al. [38]. Table I shows that our approach generally achieves the best results based on the VM and PCQI indexes. This conclusion is confirmed by careful inspection of the images presented in Fig. 6.

In summary, while existing underwater approaches are generally competitive on underwater scenes with reasonable and uniform illumination, our fusion technique demonstrates significant improvements when restoring visibility on more challenging artificially illuminated underwater scenes.

Acknowledgment

Part of this work has been funded by the Belgian NSF, and by a MOVE-IN Louvain, Marie Curie Fellowship. Part of this work has been funded from Marie Curie Actions of EU-FP7 under REA grant agreement no. 600388 (TECNIOspring programme), and from the Agency for Business Competitiveness of the Government of Catalonia ACCIO : TECSPR14-2-0023.

References

[1] Donna M. Kocak, Fraser R. Dalgleish, Frank M. Caimi, and Yoav Y. Schechner, "A focus on recent developments and trends in underwater imaging," *Marine Technology Society Journal*, 2008.
[2] B. A. Levedahl and L. Silverberg, "Control of underwater vehicles in full unsteady flow," *IEEE Journal of Oceanic Engineering*, 2009.
[3] C. H. Mazel, "In situ measurement of reflectance and fluorescence spectra to support hyperspectral remote sensing and marine biology research," *In IEEE Oceans*, 2006.
[4] G. L. Forest, "Visual inspection of sea bottom structures by an autonomous underwater vehicle," *IEEE Trans. Syst. Man and Cyber*, vol. 31, pp. 691–705, 2001.
[5] Y. Kahanov and J. Royal, "Analysis of hull remains of the dor d vessel, tantura lagoon, israel," *Int. Journal of Nautical Archeology*, 2001.
[6] D.-M. He and G. G. L. Seet, "Divergent-beam lidar imaging in turbid water," *Optics and Lasers in Engineering*, 2004.
[7] T. Treibitz and Y.Y. Schechner, "Active polarization descattering," *IEEE Trans Pattern Anal Mach Intell.*, 2009.
[8] R. T. Tan, "Visibility in bad weather from a single image," *In IEEE Conference on Computer Vision and Pattern Recognition*, 2008.
[9] K. He, J. Sun, and X. Tang, "Single image haze removal using dark channel prior," *In IEEE CVPR*, 2009.
[10] C. O. Ancuti, C. Ancuti, C. Hermans, and P. Bekaert, "A fast semi-inverse approach to detect and remove the haze from a single image," *ACCV*, 2010.
[11] C.O. Ancuti and C. Ancuti, "Single image dehazing by multi-scale fusion," *IEEE Trans. on Image Proces.*, 2013.
[12] C. Ancuti and C. O. Ancuti, "Effective contrast-based dehazing for robust image matching," *IEEE Geosc. and Remote Sensing Letter*, 2014.
[13] L. K. Choi, J. You, and A. C. Bovik, "Referenceless prediction of perceptual fog density and perceptual image defogging," *IEEE Trans. on Image Processing*, vol. 24, no. 10, 2015.
[14] C. De Vleeschouwer C. Ancuti, C. O. Ancuti and A. C. Bovik, "Night-time dehazing by fusion," *IEEE ICIP*, 2016.

	Carlevaris-B. et al.		He et al.		Drews-Jr et al.		Galdran et al.		Emberton et al.		Our method	
	VM	PCQI	VM	PCQI	VM	PCQI	VM	PCQI	VM	PCQI	VM	PCQI
Shipwreck	53.23	0.32	39.29	1.01	41.44	0.65	48.85	0.93	44.64	0.94	**49.29**	**1.10**
Fish	52.79	**1.19**	41.57	1.02	41.06	0.86	42.97	0.84	53.11	1.15	**57.39**	1.15
Reef1	76.64	1.05	69.78	1.00	80.74	1.04	72.31	0.79	**79.45**	**1.08**	74.62	1.03
Reef2	73.33	0.53	51.97	0.71	55.54	0.43	49.93	0.77	**58.63**	0.54	55.68	**1.01**
Reef3	**104.98**	0.90	63.90	0.98	83.24	0.73	71.07	0.88	89.93	0.88	79.24	**1.26**
Galdran1	70.08	0.68	69.12	1.06	71.38	0.75	69.71	0.51	**93.35**	1.15	84.71	**1.18**
Galdran9	43.73	1.10	27.91	0.98	30.64	0.86	41.81	1.16	36.13	1.14	**48.96**	**1.22**
Ancuti1	26.86	1.04	20.91	0.86	19.84	0.91	27.99	0.96	23.79	1.04	**52.65**	**1.25**
Ancuti2	13.21	0.62	17.32	0.64	17.63	0.48	24.93	0.60	16.66	0.60	**62.54**	**1.47**
Ancuti3	44.44	1.01	36.72	1.07	43.49	0.97	48.56	1.02	43.85	1.13	**64.14**	**1.25**
Average	55.93	0.84	43.85	0.93	48.50	0.77	49.81	0.85	53.95	0.96	**62.92**	**1.19**

TABLE I

Quantitative assessment of the results based on the VM and PCQI indices. Several associated images are shown in Fig. 6. From left to right we compare with the methods of Carlevaris-Bianco et al. [16], He et al. [21], Drews-Jr et al. [18], Galdran et al. [19] and Emberton et al. [20].

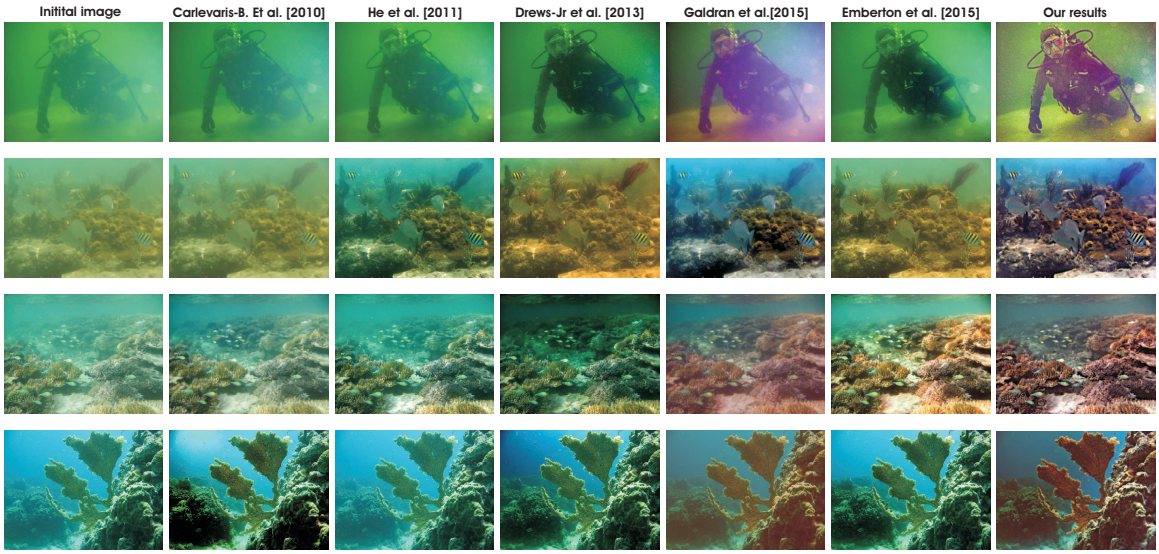

Fig. 6. ***Comparative results on underwater scenes with uniform lightning***. From a set of ten underwater images used in [20] and evaluated in Table I, the comparative results for images referred as **Ancuti2**, **Ancuti3**, **Galdran1** and **Reef1** are shown.

[15] C. Ancuti, C. O. Ancuti, T. Haber, and P. Bekaert, "Enhancing underwater images and videos by fusion," in *IEEE Conference on Computer Vision and Pattern Recognition (CVPR)*, 2012.

[16] N. Carlevaris-Bianco, A. Mohan, and R. M. Eustice, "Initial results in underwater single image dehazing," *In Proc. of IEEE OCEANS*, 2010.

[17] J. Y. Chiang and Y. Chen, "Underwater image enhancement by wavelength compensation and dehazing," *IEEE TIP*, 2012.

[18] P. Drews-Jr, E. Nascimento, F. Moraes, S. Botelho, M. Campos, and R. Grande-Brazil, "Transmission estimation in underwater single images," *IEEE Workshop ICCV*, 2013.

[19] A. Galdran, D. Pardo, A. Picon, and A. Alvarez-Gila, "Automatic red-channel underwater image restoration," *Journal of Visual Communication and Image Representation*, 2015.

[20] S. Emberton, L. Chittka, and A. Cavallaro, "Hierarchical rank-based veiling light estimation for underwater dehazing," *BMVC*, 2015.

[21] K. He, J. Sun, and X. Tang, "Single image haze removal using dark channel prior," *IEEE Trans. on Patt. Anal. and Mach. Intell.*, 2011.

[22] P. Burt and T. Adelson, "The laplacian pyramid as a compact image code," *IEEE Transactions on Communication*, vol. 31, no. 4, 1983.

[23] B. L. McGlamery, "A computer model for underwater camera systems," *Ocean Optics*, 1979.

[24] Y. Schechner and N. Karpel, "Recovery of underwater visibility and structure by polarization analysis," *IEEE J. of Oceanic Eng.*, 2005.

[25] J. N. Lythgoe and C. C. Hemmings, "Polarized light and underwater vision," *Nature*, vol. 213, no. 79, 1967.

[26] H. Koschmieder, "Theorie der horizontalen sichtweite," in *Beitrage zur Physik der freien Atmosphare*, 1924.

[27] R. Fattal, "Single image dehazing," *SIGGRAPH*, 2008.

[28] H. Kim, H. Jin, S. Hadap, and I. Kweon, "Specular reflection separation using dark channel prior," *In IEEE CVPR*, 2013.

[29] A. Agarwala, M. Dontcheva, M. Agrawala, S. M. Drucker, A. Colburn, B. Curless, D. Salesin, and M. F. Cohen, "Interactive digital photomontage," *ACM Trans. Graph (SIGGRAPH)*, 2004.

[30] P. Perez, M. Gangnet, and A. Blake, "Poisson image editing," *ACM Trans. Graph (SIGGRAPH)*, 2003.

[31] M. Grundland, R. Vohra, G. P. Williams, and N. A. Dodgson, "Cross dissolve without cross fade," *Computer Graphics Forum*, 2006.

[32] T. Mertens, J. Kautz, and Frank Van Reeth, "Exposure fusion," *Comp. Graph. Forum*, 2009.

[33] C. O. Ancuti, C. Ancuti, C. Hermans, and P. Bekaert, "Image and video decolorization by fusion," *Asian Conference on Computer Vision*, 2010.

[34] C. Ancuti and C. O. Ancuti, "Laplacian-guided image decolorization," *IEEE ICIP*, 2016.

[35] C. O. Ancuti, C. Ancuti, and P. Bekaert, "Effective single-image dehazing by fusion," in *In IEEE ICIP*, 2010.

[36] R. Achantay, S. Hemamiz, F. Estraday, and S. Susstrunk, "Frequency-tuned salient region detection," *IEEE CVPR*, 2009.

[37] D. Zhengguo, "A new visibility metric for haze images," *http://uk.mathworks.com/matlabcentral/fileexchange/33529-a-new-visibility-metric-for-haze-images*.

[38] L.S. Wang, K. Ma, and H. Yeganeh, "A patch-structure representation method for quality assessment of contrast changed images," *IEEE Signal Processing Letters*, 2015.